Environmental Science & Technology

ARTICLE

pubs.acs.org/est

Global Source−Receptor Relationships for Mercury Deposition Under Present-Day and 2050 Emissions Scenarios

Elizabeth S. Corbitt,[*,†] Daniel J. Jacob,[†,‡] Christopher D. Holmes,[§] David G. Streets,[∥] and Elsie M. Sunderland[‡,⊥]

[†]Department of Earth and Planetary Sciences, Harvard University, Cambridge, Massachusetts 02138, United States

[‡]School of Engineering and Applied Sciences, Harvard University, Cambridge, Massachusetts 02138, United States

[§]Department of Earth System Sciences, University of California Irvine, Irvine, California 92697, United States

[∥]Decision and Information Sciences Division, Argonne National Laboratory, Argonne, Illinois 60439, United States

[⊥]Department of Environmental Health, School of Public Health, Harvard University, Boston, Massachusetts 02115, United States

Supporting Information

ABSTRACT: Global policies regulating anthropogenic mercury require an understanding of the relationship between emitted and deposited mercury on intercontinental scales. Here, we examine source−receptor relationships for present-day conditions and four 2050 IPCC scenarios encompassing a range of economic development and environmental regulation projections. We use the GEOS-Chem global model to track mercury from its point of emission through rapid cycling in surface ocean and land reservoirs to its accumulation in longer lived ocean and soil pools. Deposited mercury has a local component (emitted Hg^{II}, lifetime of 3.7 days against deposition) and a global component (emitted Hg^{0}, lifetime of 6 months against deposition). Fast recycling of deposited mercury through photoreduction of Hg^{II} and re-emission of Hg^{0} from surface reservoirs (ice, land, surface ocean) increases the effective lifetime of anthropogenic mercury to 9 months against loss to legacy reservoirs (soil pools and the subsurface ocean). This lifetime is still sufficiently short that source−receptor relationships have a strong hemispheric signature. Asian emissions are the largest source of anthropogenic deposition to all ocean basins, though there is also regional source influence from upwind continents. Current anthropogenic emissions account for only about one-third of mercury deposition to the global ocean with the remainder from natural and legacy sources. However, controls on anthropogenic emissions would have the added benefit of reducing the legacy mercury re-emitted to the atmosphere. Better understanding is needed of the time scales for transfer of mercury from active pools to stable geochemical reservoirs.

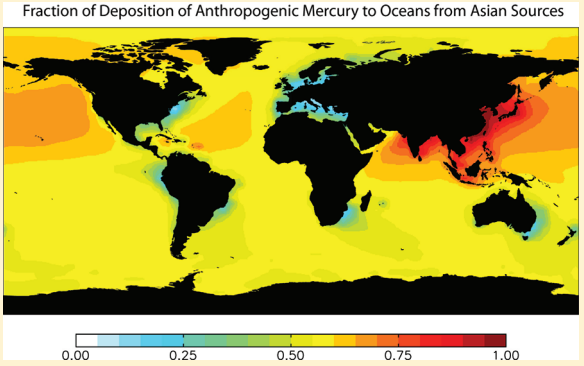

INTRODUCTION

Human activities have caused at least a 3-fold increase in atmospheric mercury deposition to terrestrial and aquatic ecosystems over the past two centuries.[1−6] Mercury bioaccumulates in freshwater and marine foodwebs with health consequences for exposed wildlife and humans.[7−9] Anthropogenic emissions are mainly from coal combustion, waste incineration, and mining.[10] Growing concern about elevated mercury in the environment has prompted negotiations under the United Nations Environment Programme (UNEP) toward a global treaty on anthropogenic mercury sources. Improving the understanding of source−receptor relationships linking mercury emissions to deposition fluxes is critical in this context. Here, we use a global atmospheric model with coupled surface reservoirs (GEOS-Chem) to quantify source−receptor relationships on continental scales for the present-day and for 2050 emission projections.

Anthropogenic activities emit mercury in both elemental (Hg^{0}) and divalent (Hg^{II}) forms. Hg^{II} is highly water soluble and can be deposited close to sources. Hg^{0} is only sparingly soluble and has an atmospheric lifetime of months against oxidation to Hg^{II}, resulting in global-scale deposition. The speciation of anthropogenic mercury varies with source type and emissions control technology. Emission controls for other pollutants, such as flue-gas desulfurization (FGD) in coal combustion, capture Hg^{II} as a cobenefit. Greater capture can be achieved with injection of chemicals to oxidize Hg^{0} to Hg^{II} or with particles designed to adsorb mercury upstream of FGDs.[11]

Projections of future anthropogenic mercury emissions out to 2050 have been reported by Streets et al.[10] on the basis of four IPCC SRES scenarios[12] spanning a range of industrial growth and environmental regulation possibilities. They find that global

Received: July 22, 2011
Accepted: November 3, 2011
Revised: October 24, 2011
Published: November 03, 2011

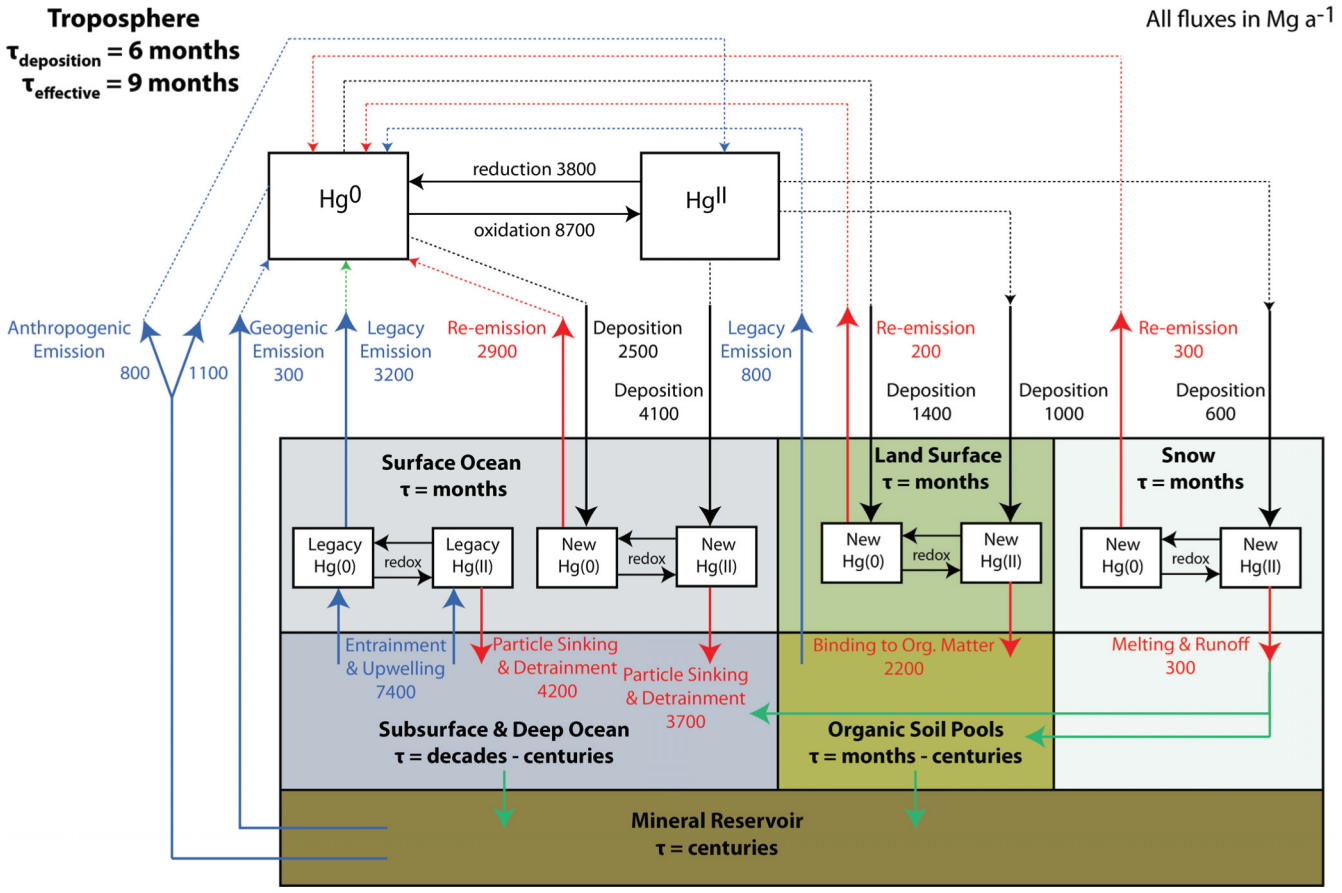

Figure 1. Global present-day budget of mercury as represented in GEOS-Chem. Blue arrows show primary and legacy sources of mercury to the atmosphere from long-lived deep reservoirs. Red arrows show the fate of mercury in surface (ocean, land, snow) reservoirs: recycling to the atmosphere or incorporation into more stable reservoirs (deep ocean, soils). Black arrows show deposition and redox fluxes. Green arrows show processes not explicitly modeled in GEOS-Chem. Order-of-magnitude residence times in individual reservoirs are also shown.

anthropogenic mercury emissions may at worst double in the future (A1B scenario) or at best stay constant (B1). Coal combustion in developing countries is the largest driver of emission increases. We examine the implications of these future scenarios for global mercury deposition and comment on the major uncertainties. There have been no studies to date that quantify future deposition for long-range IPCC scenarios. This information is needed to evaluate the effectiveness of global and national-level reductions in anthropogenic emissions on mercury deposition rates and to inform policy decisions such as the ongoing UNEP global treaty negotiations.

METHODS

General Model Description. We use the GEOS-Chem global mercury model version 8-03-02 (http://acmg.seas.harvard.edu/geos/), including a 3-D atmosphere coupled to 2-D slab ocean and terrestrial reservoirs.[13−15] We conduct simulations at 4° × 5° horizontal resolution, with 47 atmospheric levels in the vertical, using assimilated meteorological fields from the NASA Goddard Earth Observing System (GEOS-5). Following Selin et al.,[13] we first initialize the model to steady state for preindustrial conditions, and this serves to equilibrate the 2-D terrestrial reservoir. We then update the model to present day by including anthropogenic emissions, increasing terrestrial concentrations on the basis of anthropogenic deposition patterns, specifying subsurface ocean concentrations for different basins based on observations,[15−17] and conducting a simulation for 7 years to equilibrate the atmosphere. For the 2050 scenarios, we start from present-day conditions in the surface reservoirs and conduct a simulation for 7 years using future anthropogenic emissions. All results presented here are 3-year averages using 2005−2007 meteorological data.

The model used here is as described by Holmes et al.[14] with addition of a more mechanistic and resolved surface ocean model.[15] Detailed comparisons of the model to observations are presented in these two references. The model tracks three mercury forms in the atmosphere: Hg^0, Hg^{II}, and refractory particulate mercury (Hg^P). Hg^P makes a negligible (<1%) contribution to the total atmospheric burden, and we do not discuss it further. The atmospheric speciation of mercury deposited to the ocean is not relevant for aqueous chemistry as rapid reequilibration takes place in solution in open-ocean environments.[18]

Figure 1 shows the global cycling of mercury in the environment as represented by the model. "Primary" emission from mineral reservoirs through anthropogenic activities (coal combustion, industry, mining) and natural geogenic processes (weathering, volcanoes) initiates cycling between the atmosphere and surface reservoirs mediated by Hg^0/Hg^{II} redox chemistry. Redox chemistry in the atmosphere includes oxidation of

Hg^0 to Hg^{II} by Br atoms and aqueous photoreduction of Hg^{II} to Hg^0 in clouds. Dry deposition applies to both Hg^0 and Hg^{II} and wet deposition only to Hg^{II}. Uptake on sea salt particles is a major sink for Hg^{II} in the marine boundary layer.[19] Processes in the surface ocean include photochemical and biotic redox chemistry as well as sorption to particles. Mercury can be re-emitted to the atmosphere as Hg^0 or transferred to deeper ocean waters by particle sinking and vertical entrainment.[15] Hg^{II} deposited to land can be promptly photoreduced and re-emitted or bind to organic carbon and enter longer lived soil pools.[20] Hg^{II} deposited to snow can be photoreduced and re-emitted or eventually transferred to the oceans or soils through meltwater. Here, we denote anthropogenic mercury transferred from surface reservoirs to subsurface reservoirs (subsurface/deep ocean, soils) as "legacy" mercury. The current model does not explicitly resolve the recycling of this legacy mercury and instead includes it in the specification of boundary conditions.[13] We include biomass burning in our simulation but treat it as a legacy emission. Total present-day emissions from all surface reservoirs in the model, 5200 Mg a^{-1} including net ocean evasion of Hg^0, are within the range of recent estimates (3600−6300 Mg a^{-1} [16,21]).

An innovation in the current model is the tagging of mercury from source to receptor including transit through the surface reservoirs. Tagged mercury tracers for particular source regions or source types maintain their identity through transport, chemical transformation, and cycling through surface terrestrial and ocean reservoirs. Anthropogenic emissions are divided geographically into 17 world regions based on Streets et al.[10] Mercury upwelling from the subsurface ocean is divided among different ocean basins (Supporting Information, Figures 1 and 2). Geogenic (volcanoes, mineral weathering), soil, and biomass burning emissions are also separated as individual tracers.

Anthropogenic Emissions. Present-day anthropogenic emissions are based on a $1° \times 1°$ gridded, speciated inventory for the year 2005,[22] and are scaled to regional emission totals from Streets et al.[10] The magnitude of global anthropogenic emissions has an estimated uncertainty of ±30%, while chemical speciation has an uncertainty of ±20%.[10,23] Year 2050 simulations keep the fine spatial distribution of emissions the same but apply regional scaling factors projected by Streets et al.[10,23] Scaling emissions at the regional level assumes a uniform increase or decrease in emissions across all sources within each region. The projections are based on four IPCC SRES scenarios (A1B, A2, B1, B2) distinguished by their assumptions regarding industrial growth, energy policy, and emissions control. The worst-case scenario (A1B) assumes heavy use of coal with limited emission control technology, while the best-case scenario (B1) assumes aggressive transition away from fossil fuel energy sources and implementation of efficient control technology (up to 70% mercury capture in developed countries). We call these "end-member" scenarios. Scenarios A2 and B2 are intermediate and have more spatially heterogeneous trends (Supporting Information Figure 3). The speciation of emissions varies by region due to differences in sector makeup and emissions controls, from <30% Hg^{II} in South America and Northern Africa, where artisanal gold mining is a large source of Hg^0, to >60% Hg^{II} in Eastern Europe, Southern Africa, and South Asia, where power production is the largest source of emissions. Developing countries with less stringent environmental controls undergo the most growth in the future scenarios, especially in coal combustion, resulting in a greater fraction of global anthropogenic emissions as Hg^{II} in 2050 (55−60% compared to 43% in the present). Streets et al.[10] do not consider in their base projections the introduction of more advanced mercury control technology such as activated carbon injection, which is not currently commercially available, but they note that anthropogenic emissions could be as much as 30% lower in each future scenario with widespread adoption. See Supporting Information Table 1 for a summary of global emissions and deposition for the scenarios used in this study.

RESULTS AND DISCUSSION

Time Scales for Mercury Deposition. Deposition to a given region consists of a locally sourced component from emitted Hg^{II} and a background component. The mean model lifetime of Hg^0 against oxidation and deposition in the troposphere is 4 months, while the mean lifetime of boundary layer Hg^{II} against deposition is 3.7 days. One-third of emitted Hg^{II} in the model is photoreduced to Hg^0, transferring from the local to the background deposition pool. The mean model lifetime of anthropogenic Hg_T ($Hg_T \equiv Hg^0+Hg^{II}$) against deposition is 5 months, while the lifetime of Hg_T from all sources is 6 months because emissions from natural processes are as Hg^0. Re-emission of deposited mercury from surface reservoirs (Figure 1) increases the effective lifetime of anthropogenic mercury to 7 months (9 months for mercury from all sources) against incorporation into legacy organic soil and deep ocean reservoirs. The ability of GEOS-Chem to reproduce the observed atmospheric variability of Hg^0 [14] lends some confidence in these model time scales.

We refer to gross deposition as the removal of atmospheric Hg to the surface reservoirs, including wet deposition of Hg^{II} and dry deposition of Hg^0 and Hg^{II}. Some of that gross deposition is re-emitted to the atmosphere as Hg^0, and we refer to the remainder as net deposition, balanced by transfer to deeper reservoirs (Figure 1). We view net deposition as the metric for mercury enrichment in ecosystems, balancing primary emissions on a global scale. Our tracking of mercury through surface reservoirs in GEOS-Chem enables us to relate net deposition to the original emission source. The 9-month lifetime of atmospheric Hg^0 against transfer to the legacy reservoirs (i.e., accounting for reduction and re-emission from the surface reservoirs) is shorter than the time scale for interhemispheric exchange (~1 year[24]), which means that a strong hemispheric signature is to be expected in source−receptor relationships even for the background component of mercury.

Figure 2 shows annual mean gross and net deposition fluxes in the model for present-day conditions. Gross deposition peaks over polluted continents due to emitted Hg^{II} and over windy regions of the oceans due to high Br concentrations and fast sea-salt deposition. The fraction of deposited mercury that is re-emitted rather than transferred to the deeper reservoirs is 10% for land, 40% for the oceans, and 50% for snow. Most of the mercury deposited to land enters the soil pools where it has an estimated mean lifetime of 80 years against re-emission by soil respiration[20] and is included here as a legacy source. By contrast, mercury deposited to the surface ocean has a lifetime of only 6 months against re-emission, competing with transfer to the subsurface ocean (lifetime of 5 months). Net deposition of mercury in the model thus tends to be higher over land than over oceans.

Global Source−Receptor Relationships. We define the source−receptor influence function I_{ij} for mercury deposition as

$$I_{ij} = D_{ij}/E_i \quad (1)$$

where D_{ij} is the net deposition flux to receptor region j from emissions in region i and E_i is the total emission rate for region i.

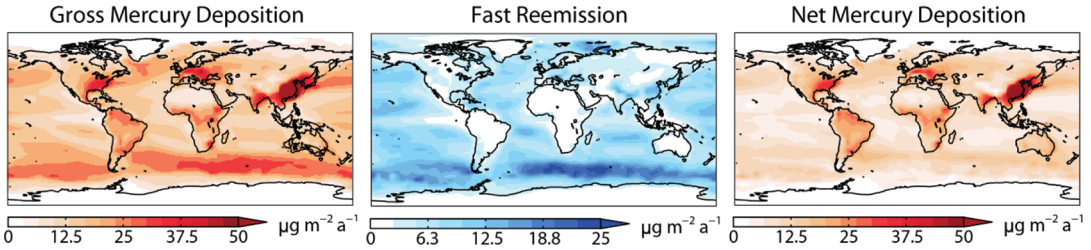

Figure 2. Annual mean mercury deposition and fast re-emission from surface reservoirs simulated by GEOS-Chem for present-day conditions. Fast re-emission from surface reservoirs competes with transfer to longer lived reservoirs. Net deposition is the balance between gross deposition and fast re-emission.

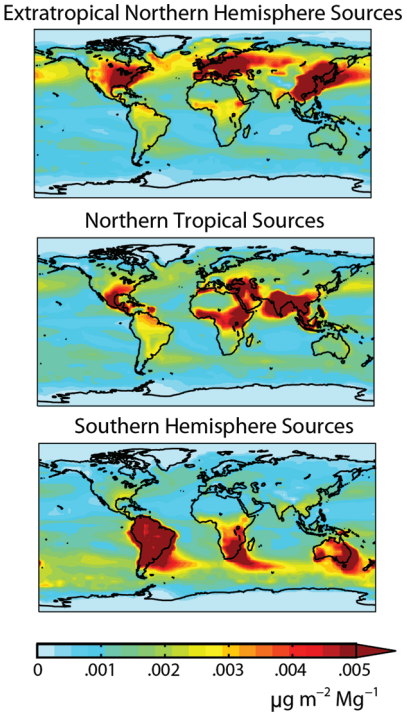

Figure 3. Influence functions for anthropogenic mercury emitted from source regions in three latitudinal bands: extratropical Northern Hemisphere (Canada, United States, Europe, Russia, East Asia), northern tropics (Central America, Northern Africa, Middle East, South Asia, Southeast Asia), and Southern Hemisphere (South America, Southern Africa, Australia). Maps show the preferential locations for deposition of mercury emitted from each latitudinal band, normalized to the magnitude of emissions as given by eq 1.

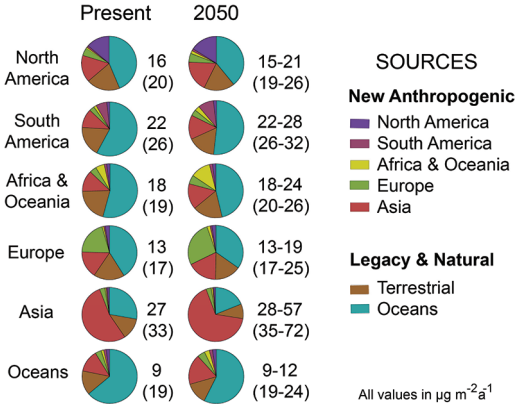

Figure 4. Sources of mercury deposited to aggregated world regions for the present-day and for the four 2050 IPCC scenarios of Streets et al.[10] Numbers give annual net deposition fluxes to the receptor region (gross deposition fluxes in parentheses) and for 2050 represent the range of the IPCC scenarios. Pie charts show relative source contributions to deposition (average of the scenarios for 2050). "New anthropogenic" refers to mercury from primary emissions (coal combustion, waste incineration, mining) including recycling through surface reservoirs (ocean mixed layer, vegetation). "Legacy" refers to anthropogenic mercury recycled from intermediate reservoirs with a time scale of decades or longer and included in GEOS-Chem as boundary condition.

This influence function enables us to evaluate where, gram-for-gram, emissions reductions would be most effective to reduce deposition to a given region. Figure 3 shows influence functions for anthropogenic emissions in the extra-tropical Northern Hemisphere, the northern tropics, and the Southern Hemisphere. We find that extra-tropical sources make a particularly large contribution to deposition within their hemisphere. Emissions in the tropics have a more distributed influence. See Supporting Information Figure 4 for additional maps of influence functions by individual source regions. Supporting Information Figure 5 shows the fraction of total deposition attributed to anthropogenic sources from each region.

Figure 4 shows the source attribution for mercury deposited to aggregated world regions under present-day and 2050 emissions. Constraints from sediment and ice cores and from current anthropogenic emission inventories imply that deposition on a global scale is approximately one-third natural, one-third legacy anthropogenic, and one-third primary anthropogenic.[1,5,6,21] Natural and legacy mercury emissions from terrestrial soils and oceans contribute the majority of net deposition in all regions except Asia, stressing the importance of better resolving the legacy component in future work. For example, it is thought that Hg^0 evasion in the North Atlantic Ocean is presently enhanced due to enrichment of subsurface seawater by legacy anthropogenic sources.[15,16] North America is likely the strongest contributor to this enrichment due to its high influence function and very high emissions from mining in the late 19th century.[25,26]

Mercury deposition in 2050 relative to present day is similar in the B1 scenario but increases in the other IPCC scenarios, reflecting the global trend in emissions.[10] The increasing Hg^{II} fraction of total mercury emissions in the future results in an increasing relative domestic contribution to deposition. This is most apparent in Asia, where the fraction of mercury deposition from domestic anthropogenic sources increases from 54% in the present day to 56−75% in 2050. Natural and legacy emissions are assumed here to stay constant between present day and 2050,

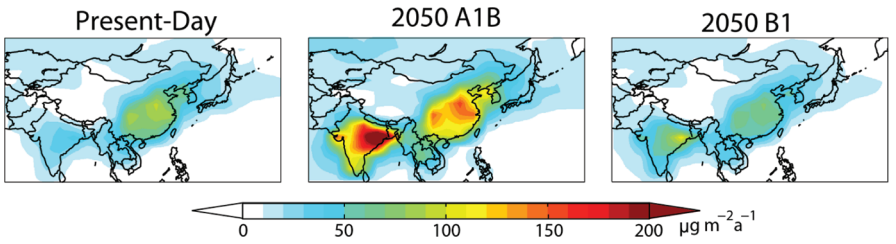

Figure 5. Annual mean net mercury deposition fluxes to Asia for the present-day and end-member IPCC 2050 scenarios.

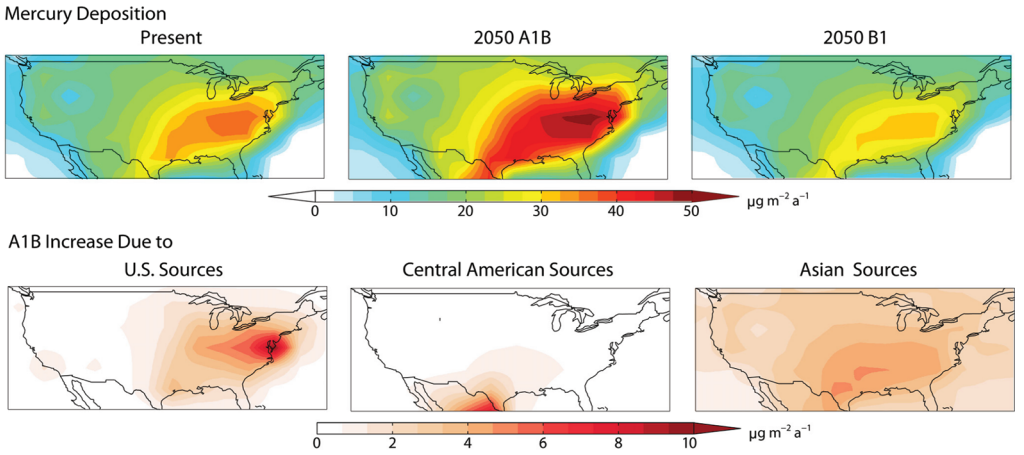

Figure 6. (Top panels) Annual mean net mercury deposition flux to the United States for present-day and 2050 A1B and B1 scenarios. (Bottom panels) Changes in the source contributions from anthropogenic emissions in the United States, Central America, and Asia in the A1B 2050 scenario relative to present day.

and as a result their relative contribution to deposition decreases in 2050 for all receptor regions. This is likely an incorrect assumption as legacy emissions should increase in concert with future increases in anthropogenic emissions.

Asian emissions (mostly from China and India) account for over one-half of global anthropogenic emissions in all 2050 scenarios, and the magnitude of their projected change relative to present spans from near constant to a 240% increase. However, it is important to distinguish between China and India, as increases in India are much larger due to considerable growth in coal combustion. Figure 5 shows net deposition to Asia for the present-day and for the end-member 2050 scenarios. Deposition in China and downwind increases in the A scenarios but declines in the B scenarios due to emission controls. Deposition to India and downwind increases in all 2050 scenarios and is consistently the highest in the world. Even installation of FGD in 95% of Indian power plants in the B1 scenario is insufficient to decrease deposition levels relative to present day. Decreasing deposition to South Asia would require emissions controls specifically targeting mercury capture.

Mercury Deposition to the United States in 2050. Figure 6 shows present-day and 2050 simulated deposition fluxes of mercury to the contiguous United States. Components of present-day deposition include domestic anthropogenic emissions (17%), foreign anthropogenic emissions (23%), and natural and legacy terrestrial and ocean mercury (60%). This is similar to the previous GEOS-Chem source attribution of Selin and Jacob.[27] In the 2050 A1B scenario, both the background and the local components of deposition increase as global anthropogenic mercury emissions more than double and North American emissions increase by 60%. We find a mean 30% increase in mercury deposition rates for the United States, less than the increase in emissions because we assume no change in the natural and legacy components. The bottom panels of Figure 6 show the increase in source contributions to U.S. mercury deposition in the 2050 A1B scenario relative to present day. U.S. sources account for most of the increase in the Northeast, while Central American emissions (including Mexico) are important mainly in Texas. The increase in Asian emissions enhances net deposition more uniformly across the country but most strongly in the Southeast, reflecting both the vegetation density (enhancing dry deposition) and the deep convective precipitation scavenging of Hg^{II} from the upper troposphere.[27,28] Though South Asian sources (mainly India) undergo the most dramatic growth in A1B, we find that their impact on U.S. deposition is less than that of East Asian sources (mainly China) because of their lower latitude. In the B1 scenario, U.S. anthropogenic emissions decrease by 38% for both Hg^0 and Hg^{II}. Global emissions are similar in magnitude to the present day but shift southward and are therefore less efficient contributors to U.S. deposition. Thus, 2050 mercury deposition to the United States decreases by 10% on average and by up to 22% in the Northeast.

East Asian emissions contribute to deposition in the United States primarily by elevating background concentrations[29,30] rather than by direct intercontinental transport of short-lived Hg^{II} species. We find that only 6% of present-day East Asian deposition to the United States is from direct trans-Pacific transport

of Hg^{II}, though the share can be up to 25% in the Pacific Northwest and Alaska. East Asian total emissions increase by 47% in the A1B scenario, but the East Asian contribution to deposition in the United States only increases by 35% because most of the emissions increase is as Hg^{II}. Gram-for-gram, emissions from Russia and Eastern Europe are more efficiently transported to the United States because of re-emission of mercury deposited to snow during transport over the Arctic.

Model Uncertainties. There are a range of uncertainties involved in global mercury modeling,[31−34] some of which are especially relevant to our understanding of global source−receptor relationships. One important uncertainty is the atmospheric reduction of emitted Hg^{II}. On a global scale, the rate of Hg^{II} reduction must be relatively slow, as implied by constraints from the observed seasonal variation of Hg^0 and the atmospheric variability of Hg_T.[14,35] We conduct a sensitivity simulation with no Hg^{II} reduction and with Hg^0 oxidation rates correspondingly adjusted to match observational constraints on Hg^0 concentrations and find no major effects on the results reported here. More details are available in the Supporting Information. However, there is some evidence for fast Hg^{II} reduction taking place in coal combustion plumes.[36−39] This reduction would decrease the local component of regional deposition in our simulation. The associated error is difficult to quantify because the mechanism for Hg^{II} reduction in fresh plumes is unknown.[36]

Regardless of the fate of primary Hg^{II}, an important result of our work is the latitudinal structure of source−receptor relationships for mercury, i.e., emissions have the greatest effect on deposition in their latitudinal band (Figure 3). This follows from the atmospheric lifetime of Hg_T against deposition, which is constrained by observation of Hg_T atmospheric variability.[40,41] There is presently discussion in the literature as to whether atmospheric oxidation of Hg^0, determining Hg_T deposition, involves Br atoms or OH and O_3.[14,42,43] Our standard simulations uses Br atoms, and we conduct a sensitivity simulation using OH and O_3 as described by Holmes et al.[14] We find that in the base simulation net deposition to midlatitude regions is similar, while deposition is lower in the tropics and higher in polar regions. This is consistent with recent findings from an intercomparison of six mercury models for the Task Force on Hemispheric Transport of Air Pollution.[31] Differences in modeled deposition are greatest where measurements are sparsest. Additional long-term monitoring stations in the Arctic and tropics would help constrain the atmospheric oxidant of Hg^0. The source attribution of regional deposition remains essentially unchanged because deposition to a receptor region is most influenced by sources in the same broad latitudinal bands.

Another issue is the fate of mercury in the surface reservoirs following deposition. Isotopic observations place constraints on the extent of fast recycling of mercury deposited to land,[44−46] but additional study is needed to characterize differences across multiple ecosystem types. The fraction of mercury deposited to oceans that is re-emitted to the atmosphere (40% in our standard simulation) depends on redox kinetics in the surface ocean and the size of the reducible Hg^{II} pool. Although redox kinetics for characterizing the net reduction of Hg^{II} to Hg^0 in the surface ocean represent a major uncertainty,[47] our simulation uses rate constants constrained by experimental data using stable Hg isotopes.[48] The size of the reducible pool is highly uncertain and depends on partitioning to particulate organic carbon as well as formation of stable inorganic complexes in solution that are resistant to reduction.[48] In our model parametrization 40% of dissolved Hg^{II} is available for reduction.[15] This is the lower bound from measurements in freshwater ecosystems (40−60%);[48,49] however, no data are available for marine ecosystems. Ocean re-emissions increase or decline proportionally to the reducible Hg^{II} pool size. To address this uncertainty, evasion rates for the standard simulation have has been optimized to best match observational constraints for atmospheric and seawater Hg^0 concentrations.[15] We model Hg^{II} partitioning to particles and removal from the surface ocean based on variability in biological productivity and ocean export fluxes. Modeled air−sea exchange is also sensitive (±30%) to the evasion scheme employed.[50−52] Though the magnitude of evasion varies across schemes, the fraction of mercury from the subsurface ocean vs atmospheric deposition is unaffected, so source attribution is unchanged. Additional study of the redox kinetics of different Hg^{II} complexes in marine waters as well as coupled cycling in association with organic carbon in the global oceans would improve our understanding of the lifetime of Hg in actively cycling reservoirs and the time scales for sequestering anthropogenic mercury in deep ocean reservoirs.

Implications for Policy. Separation of source contributions to mercury deposition between a local component from emitted Hg^{II} and a background component from emitted Hg^0 allows a simplified estimate of source−receptor relationships on continental scales. We used GEOS-Chem for the present-day and 2050 simulations to construct a best-fit linear regression model relating net deposition fluxes in a region i (D_i) to the regional emission of Hg^{II} ($E_{i\ HgII}$) and to the global emission of Hg^0 (E_{Hg0}). We find the following form (r^2 = 0.91, Supporting Information, Figure 7)

$$D_i = 0.39E_{iHgII} + 0.74E_{Hg0} + 10 \quad (2)$$

where all values are in $\mu g\ m^{-2}\ a^{-1}$. The 0.39 coefficient for $E_{i\ HgII}$ represents the average fraction of regional Hg^{II} emissions that deposits within the region and is not quickly re-emitted. The intercept of 10 $\mu g\ m^{-2}\ a^{-1}$ represents the mean deposition from natural and legacy terrestrial sources. This linear regression assumes that all Hg^0 emitted worldwide is equally efficient in contributing to deposition in a given receptor region, and this is not correct (see Figure 4 and related discussion). The simple regression equation still performs well in most regions, with a mean residual of 4 $\mu g\ m^{-2}\ a^{-1}$. Supporting Information Figure 6 shows the major exporters of anthropogenic mercury by region.

Humans are exposed to mercury through commercial fish caught in oceans worldwide.[9] A combination of both decreases in deposition to local ecosystems and global oceans is therefore needed to most effectively reduce exposures and risks. Asia presently contributes more than one-half of new anthropogenic deposition to all ocean basins (from 53% to the North Atlantic to 62% to the North Pacific) because it represents such a large global source; its contribution is expected to further grow in the future. North American and European sources contribute 30% of new anthropogenic deposition to the North Atlantic and less in other ocean basins. However, two-thirds of present-day deposition to the ocean is from natural and legacy sources, and much of the legacy anthropogenic mercury is due to North American and European emissions from the past two centuries.[25]

Present-day primary anthropogenic emissions contribute only about one-third of global mercury deposition, and this has been used to argue that future emission controls would have relatively little impact. This perspective is flawed in that it does not

recognize that future emissions also increase the mercury stored in legacy pools. On time scales of decades to centuries, the legacy mercury presently in organic soils and subsurface ocean waters will enter more geochemically stable reservoirs in deep ocean sediments and recalcitrant soil pools.[16,20] Thus, mercury currently in the legacy pools will decline over time unless new emissions restore it. The benefit of decreasing primary anthropogenic emissions must therefore factor in the resulting decrease in re-emission of mercury from legacy pools. This is similar to the CO_2 problem in that emitted CO_2 has an atmospheric lifetime of only 5 years against uptake by the ocean and land but is re-emitted multiple times from these surface reservoirs. The effective legacy of emitted CO_2 (expressed by the IPCC as global warming potential) is more than a century.[53] In the same way, the effect of anthropogenic mercury emissions should be viewed in terms of their long-term legacy. This calls for better understanding of the time scales associated with mercury in legacy pools and its transfer to geochemically stable reservoirs.

■ ASSOCIATED CONTENT

Supporting Information. Additional information, including more information on emissions scenarios, sensitivity analysis, and additional figures. This material is available free of charge via the Internet at http://pubs.acs.org.

■ AUTHOR INFORMATION

Corresponding Author
*Phone: (617) 384-7835; e-mail: corbitt@seas.harvard.edu.

■ ACKNOWLEDGMENT

We acknowledge financial support for this study from the NSF Atmospheric Chemistry Program, the EPA STAR program, and Electric Power Research Institute (EPRI). E.S.C. acknowledges support from the NSF graduate fellowship program. E.M.S. acknowledges new investigator support from the HSPH-NIEHS Center for Environmental Health. We thank Helen Amos for helpful discussions.

■ REFERENCES

(1) Lamborg, C. H.; Fitzgerald, W. F.; Damman, A. W. H.; Benoit, J. M.; Balcom, P. H.; Engstrom, D. R. Modern and historic atmospheric mercury fluxes in both hemispheres: Global and regional mercury cycling implications. *Global Biogeochem. Cycles* **2002**, *16* (4).

(2) Fitzgerald, W. F.; Engstrom, D. R.; Mason, R. P.; Nater, E. A. The case for atmospheric mercury contamination in remote areas. *Environ. Sci. Technol.* **1998**, *32* (1), 1.

(3) Schuster, P. F.; Krabbenhoft, D. P.; Naftz, D. L.; Cecil, L. D.; Olson, M. L.; Dewild, J. F.; Susong, D. D.; Green, J. R.; Abbott, M. L. Atmospheric mercury deposition during the last 270 years: A glacial ice core record of natural and anthropogenic sources. *Environ. Sci. Technol.* **2002**, *36* (11), 2303.

(4) Roos-Barraclough, F.; Martinez-Cortizas, A.; Garcia-Rodeja, E.; Shotyk, W. A 14 500 year record of the accumulation of atmospheric mercury in peat: volcanic signals, anthropogenic influences and a correlation to bromine accumulation. *Earth Planet. Sci. Lett.* **2002**, *202* (2), 435.

(5) Fitzgerald, W. F.; Engstrom, D. R.; Lamborg, C. H.; Tseng, C. M.; Balcom, P. H.; Hammerschmidt, C. R. Modern and historic atmospheric mercury fluxes in northern Alaska: Global sources and Arctic depletion. *Environ. Sci. Technol.* **2005**, *39* (2), 557.

(6) Hermanson, M. H. Historical accumulation of atmospherically derived pollutant trace-metals in the Arctic as measured in dated sediment cores. *Water Sci. Technol.* **1993**, *28* (8−9), 33.

(7) In *Ecotoxicology of mercury*, 2nd ed.; Wiener, J. G., Krabbenhoft, D. P., Heinz, G. H., Scheuhammer, A. M., Eds.; CRC Press: Boca Raton, FL, 2003.

(8) Clarkson, T. W.; Magos, L. The toxicology of mercury and its chemical compounds. *Crit. Rev. Toxicol.* **2006**, *36* (8), 609.

(9) Sunderland, E. M. Mercury exposure from domestic and imported estuarine and marine fish in the US seafood market. *Environ. Health Perspect.* **2007**, *115* (2), 235.

(10) Streets, D. G.; Zhang, Q.; Wu, Y. Projections of Global Mercury Emissions in 2050. *Environ. Sci. Technol.* **2009**, *43* (8), 2983.

(11) Strivastava, R. Control of mercury emissions from coal-fired electric utility boilers: An update. U.S. Environmental Protection Agency: Research Triangle Park, NC, 2010.

(12) In *Special Report on Emissions Scenarios: A Special Report of Working Group III of the Intergovernmental Panel on Climate Change*; Nakicenovic, N., Alcamo, J., Davis, G., Eds.; Cambridge University Press: Cambridge, U.K., 2000.

(13) Selin, N. E.; Jacob, D. J.; Yantosca, R. M.; Strode, S.; Jaegle, L.; Sunderland, E. M. Global 3-D land-ocean-atmosphere model for mercury: present-day versus preindustrial cycles and anthropogenic enrichment factors for deposition. *Global Biogeochem. Cycles* **2008**, *22* (2), GB2011.

(14) Holmes, C. D.; Jacob, D. J.; Corbitt, E. S.; Mao, J.; Yang, X.; Talbot, R.; Slemr, R. Global atmospheric model for mercury including oxidation by bromine atoms. *Atmos. Chem. Phys.* **2010**, *10* (24), 12037.

(15) Soerensen, A. L.; Sunderland, E. M.; Holmes, C. D.; Jacob, D. J.; Yantosca, R. M.; Skov, H.; Christensen, J. H.; Strode, S. A.; Mason, R. P. An Improved Global Model for Air-Sea Exchange of Mercury: High Concentrations over the North Atlantic. *Environ. Sci. Technol.* **2010**, *44* (22), 8574.

(16) Sunderland, E. M.; Mason, R. P. Human impacts on open ocean mercury concentrations. *Global Biogeochem. Cycles* **2007**, *21* (4), 15.

(17) Sunderland, E. M.; Krabbenhoft, D. P.; Moreau, J. W.; Strode, S. A.; Landing, W. M. Mercury sources, distribution, and bioavailability in the North Pacific Ocean: Insights from data and models. *Global Biogeochem. Cycles* **2009**, *23*.

(18) Fitzgerald, W. F.; Lamborg, C. H.; Hammerschmidt, C. R. Marine biogeochemical cycling of mercury. *Chem. Rev.* **2007**, *107* (2), 641.

(19) Holmes, C. D.; Jacob, D. J.; Mason, R. P.; Jaffe, D. A. Sources and deposition of reactive gaseous mercury in the marine atmosphere. *Atmos. Environ.* **2009**, *43* (14), 2278.

(20) Smith-Downey, N. V.; Sunderland, E. M.; Jacob, D. J. Anthropogenic impacts on global storage and emissions of mercury from terrestrial soils: Insights from a new global model. *J. Geophys. Res.-Biogeosci.* **2010**, *115*.

(21) Pirrone, N.; Cinnirrella, S.; Feng, X.; Friedli, H.; Levin, L.; Pacyna, J.; Pacyna, E. G.; Streets, D. G.; Sundseth, K. *Mercury: Emissions*. HTAP 2010 Assessment Report, 2010.

(22) Pacyna, E. G.; Pacyna, J. M.; Sundseth, K.; Munthe, J.; Kindbom, K.; Wilson, S.; Steenhuisen, F.; Maxson, P. Global emission of mercury to the atmosphere from anthropogenic sources in 2005 and projections to 2020. *Atmos. Environ.* **2010**, *44* (20), 2487.

(23) Pacyna, E. G.; Pacyna, J. M.; Fudala, J.; Strzelecka-Jastrzab, E.; Hlawiczka, S.; Panasiuk, D. Mercury emissions to the atmosphere from anthropogenic sources in Europe in 2000 and their scenarios until 2020. *Sci. Total Environ.* **2006**, *370* (1), 147.

(24) Jacob, D. J.; Prather, M. J.; Wofsy, S. C.; McElroy, M. B. Atmospheric distribution of Kr-85 simulated with a general-circulation model. *J. Geophys. Res.-Atmos.* **1987**, *92* (D6), 6614.

(25) Streets, D. G.; Devane, M. K.; Lu, Z.; Bond, T. C.; Sunderland, E. M.; Jacob, D. J. All-time releases of mercury to the atmosphere from human activities. Submitted for publication.

(26) Pirrone, N.; Allegrini, I.; Keeler, G. J.; Nriagu, J. O.; Rossmann, R.; Robbins, J. A. Historical atmospheric mercury emissions and

depositions in North America compared to mercury accumulations in sedimentary records. *Atmos. Environ.* **1998**, *32* (5), 929.

(27) Selin, N. E.; Jacob, D. J. Seasonal and spatial patterns of mercury wet deposition in the United States: Constraints on the contribution from North American anthropogenic sources. *Atmos. Environ.* **2008**, *42* (21), 5193.

(28) Guentzel, J. L.; Landing, W. M.; Gill, G. A.; Pollman, C. D. Processes influencing rainfall deposition of mercury in Florida. *Environ. Sci. Technol.* **2001**, *35* (5), 863.

(29) Jaffe, D.; Strode, S. Sources, fate and transport of atmospheric mercury from Asia. *Environ. Chem.* **2008**, *5* (2), 121.

(30) Lin, C. J.; Pan, L.; Streets, D. G.; Shetty, S. K.; Jang, C.; Feng, X.; Chu, H. W.; Ho, T. C. Estimating mercury emission outflow from East Asia using CMAQ-Hg. *Atmos. Chem. Phys.* **2010**, *10* (4), 1853.

(31) Travnikov, O.; Lin, C.-J.; Dastoor, A.; Bullock, O. R.; Hedgecock, I. M.; Holmes, C. D.; Ilyin, I.; Jaegle, L.; Jun, G.; Pan, L.; Pongrueksa, P.; Ryzhkov, A.; Seigneur, C.; Skov, H. *Mercury: Global and Regional Modeling*; HTAP 2010 Assessment Report, 2010.

(32) Lin, C. J.; Pongprueksa, P.; Lindberg, S. E.; Pehkonen, S. O.; Byun, D.; Jang, C. Scientific uncertainties in atmospheric mercury models I: Model science evaluation. *Atmos. Environ.* **2006**, *40* (16), 2911.

(33) Ryaboshapko, A.; Bullock, O. R.; Christensen, J.; Cohen, M.; Dastoor, A.; Ilyin, I.; Petersen, G.; Syrakov, D.; Travnikov, O.; Artz, R. S.; Davignon, D.; Draxler, R. R.; Munthe, J.; Pacyna, J. Intercomparison study of atmospheric mercury models: 2. Modelling results vs. long-term observations and comparison of country deposition budgets. *Sci. Total Environ.* **2007**, *377* (2−3), 319.

(34) Bullock, O. R.; Atkinson, D.; Braverman, T.; Civerolo, K.; Dastoor, A.; Davignon, D.; Ku, J. Y.; Lohman, K.; Myers, T. C.; Park, R. J.; Seigneur, C.; Selin, N. E.; Sistla, G.; Vijayaraghavan, K. An analysis of simulated wet deposition of mercury from the North American Mercury Model Intercomparison Study. *J. Geophy. Res.-Atmos.* **2009**, *114*, 12.

(35) Selin, N. E.; Jacob, D. J.; Park, R. J.; Yantosca, R. M.; Strode, S.; Jaegle, L.; Jaffe, D. Chemical cycling and deposition of atmospheric mercury: Global constraints from observations. *J. Geophys. Res.-Atmos.* **2007**, *112* (D2), 14.

(36) Lohman, K.; Seigneur, C.; Edgerton, E.; Jansen, J. Modeling mercury in power plant plumes. *Environ. Sci. Technol.* **2006**, *40* (12), 3848.

(37) Seigneur, C.; Karamchandani, P.; Vijayaraghavan, K.; Lohman, K.; Shia, R. L.; Levin, L. On the effect of spatial resolution on atmospheric mercury modeling. *Sci. Total Environ.* **2003**, *304* (1−3), 73.

(38) Ter Schur, A.; Caffrey, J.; Gustin, M.; Holmes, C.; Hynes, A.; Landing, B.; Landis, M.; Laudel, D.; Levin, L.; Nair, U.; Jansen, J.; Ryan, J.; Walters, J.; Schauer, J.; Volkamer, R.; Waters, D.; Weiss-Penzias, P. An integrated approach to assess elevated mercury wet deposition and concentrations in the southeastern United States. *10th International Conference on Mercury as a Global Pollutant*; Halifax, NS, Canada, 2011.

(39) Edgerton, E. S.; Hartsell, B. E.; Jansen, J. J. Mercury speciation in coal-fired power plant plumes observed at three surface sites in the southeastern US. *Environ. Sci. Technol.* **2006**, *40* (15), 4563.

(40) Slemr, F.; Schuster, G.; Seiler, W. Distribution, speciation, and budget of atmospheric mercury. *J. Atmos. Chem.* **1985**, *3* (4), 407.

(41) Lin, C. J.; Pehkonen, S. O. The chemistry of atmospheric mercury: a review. *Atmos. Environ.* **1999**, *33* (13), 2067.

(42) Dastoor, A. P.; Larocque, Y. Global circulation of atmospheric mercury: a modelling study. *Atmos. Environ.* **2004**, *38* (1), 147.

(43) Seigneur, C.; Lohman, K. Effect of bromine chemistry on the atmospheric mercury cycle. *J. Geophys. Res.-Atmos.* **2008**, *113* (D23).

(44) Hintelmann, H.; Harris, R.; Heyes, A.; Hurley, J. P.; Kelly, C. A.; Krabbenhoft, D. P.; Lindberg, S.; Rudd, J. W. M.; Scott, K. J.; St Louis, V. L. Reactivity and mobility of new and old mercury deposition in a Boreal forest ecosystem during the first year of the METAALICUS study. *Environ. Sci. Technol.* **2002**, *36* (23), 5034.

(45) Graydon, J. A.; St Louis, V. L.; Lindberg, S. E.; Hintelmann, H.; Krabbenhoft, D. P. Investigation of mercury exchange between forest canopy vegetation and the atmosphere using a new dynamic chamber. *Environ. Sci. Technol.* **2006**, *40* (15), 4680.

(46) Graydon, J. W.; Zhang, X. Z.; Kirk, D. W.; Jia, C. Q. Sorption and stability of mercury on activated carbon for emission control. *J. Hazard. Mater.* **2009**, *168* (2−3), 978.

(47) Qureshi, A.; MacLeod, M.; Hungerbuhler, K. Quantifying uncertainties in the global mass balance of mercury. *Global Biogeochem, Cycles*, in press.

(48) Whalin, L.; Kim, E. H.; Mason, R. Factors influencing the oxidation, reduction, methylation and demethylation of mercury species in coastal waters. *Mar. Chem.* **2007**, *107* (3), 278.

(49) O'Driscoll, N. J.; Siciliano, S. D.; Lean, D. R. S.; Amyot, M. Gross photoreduction kinetics of mercury in temperate freshwater lakes and rivers: Application to a general model of DGM dynamics. *Environ. Sci. Technol.* **2006**, *40* (3), 837.

(50) Rolfhus, K. R.; Fitzgerald, W. F. Mechanisms and temporal variability of dissolved gaseous mercury production in coastal seawater. *Mar. Chem.* **2004**, *90* (1−4), 125.

(51) Sunderland, E. M.; Dalziel, J.; Heyes, A.; Branfireun, B. A.; Krabbenhoft, D. P.; Gobas, F. Response of a Macrotidal Estuary to Changes in Anthropogenic Mercury Loading between 1850 and 2000. *Environ. Sci. Technol.* **2010**, *44* (5), 1698.

(52) Andersson, M. E.; Gardfeldt, K.; Wangberg, I.; Sprovieri, F.; Pirrone, N.; Lindqvist, O. Seasonal and daily variation of mercury evasion at coastal and off shore sites from the Mediterranean Sea. *Mar. Chem.* **2007**, *104* (3−4), 214.

(53) Solomon, S. D.; Qin, M.; Manning, Z.; Chen, M.; Marquis, K. B.; Averyt, M. T.; Miller, H. L. *IPCC Fourth Assessment Report (AR4) Climate Change 2007: The Physical Science Basis*; Cambridge University Press: Cambridge, New York, 2007.

Supporting Information

Tagged Simulation Regions

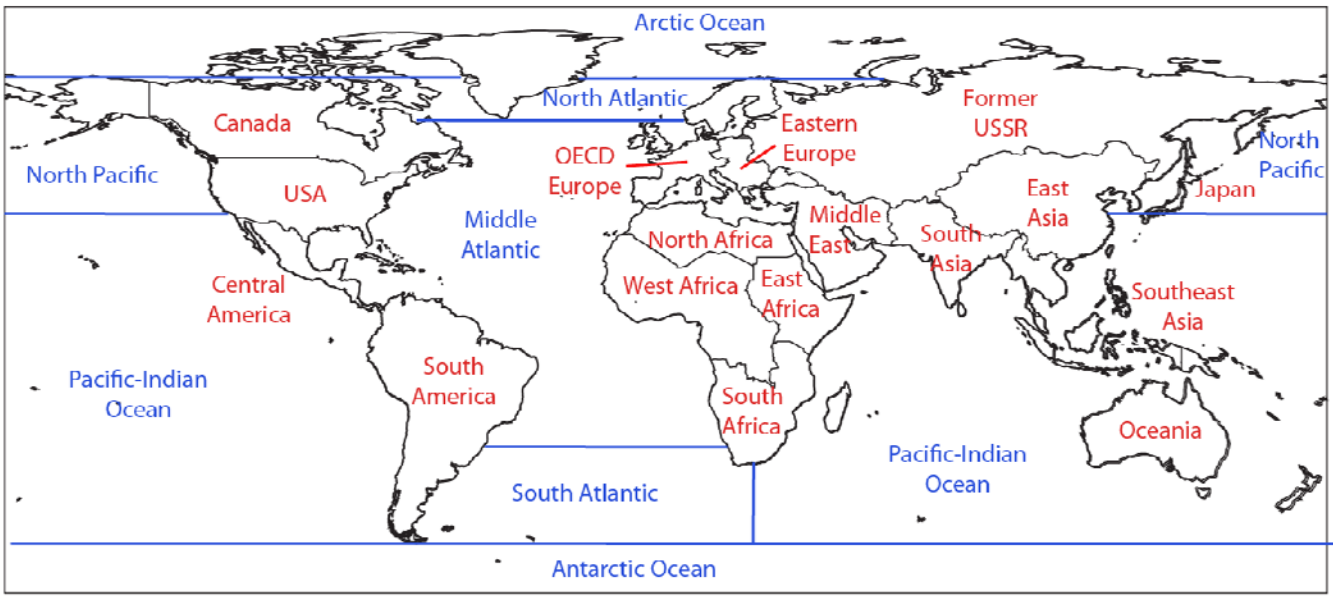

SI Figure 1 Definition of source and receptor regions: 17 anthropogenic emissions regions are from IMAGE 2.2 and are used in Streets et al. (1); 7 ocean regions from Soerensen et al. (2).

Emissions Scenarios

Our simulations are based on the mercury emissions projections by Streets et al. (1) for four IPCC scenarios of economic and technologic development (A1B, A2, B1, B2). Global economic growth is expected in all scenarios, though at a faster pace in the A scenarios. Globalization in the A1B and B1 scenarios is associated with widely distributed economic growth. Developmental paths diverge more in the A2 and B2 scenarios, with relatively more growth in already advanced industrialized countries. In all scenarios, coal-fired power production, especially in Asia, drives the largest changes in mercury emissions. In the A scenarios, industrialized countries aggressively use emissions control technology but implementation is variable among developing countries and removal efficiency is capped at the present-day level (40%). In the B scenarios, emissions controls are extended to more regions, and technology improves to 52-70% removal efficiency.

Streets et al. (1) use flue-gas desulfurization (FGD) as a proxy for all mercury emission control technologies, and adjust assumptions about capture efficiency and technological penetration in developing countries for each scenario. Even without regulation targeted specifically at mercury emission, FGD may be installed to limit emission of other air pollutants and will capture mercury as a co-benefit.

SI Table 1 (next page) Present and future (2050) global mercury emissions and deposition and fraction of deposition from regional sources (f_d). Emissions are from Streets et al. (1), modified to include emissions from fuel combustion and industrial processes only, i.e. does not include biomass burning. Deposition is gross downward flux and is greater than the sum of anthropogenic and non-varying natural and historical emissions (6100 Mg/y) due to recycling in the surface ocean, vegetation, and snow reservoirs. Annual emissions and deposition are rounded to the nearest hundred Mg. We calculate f_d as the fraction of total deposition in a model grid box that originates from anthropogenic sources in the same world region.

Scenario	Description	Anthropogenic Emissions (Mg a^{-1})	Gross Total Deposition (Mg a^{-1})	f_d (%) Gross	f_d (%) Net
Present-day	Sectors: Industrial processes 53% Power plant combustion 24% Residential/industrial fuel 23% Speciation: 57% $Hg^{0,}$ 37% Hg^{II}, 6% Hg^{P} 40% removal efficiency Largest anthro: East Asia 51%, USA 7%	1900	9600	10.4	9.3
2050 A1B	Sectors: Industrial processes 24% Power plant combustion 56% Residential/industrial fuel 20% Speciation: 40% Hg^{0}, 55% Hg^{II}, 5% Hg^{P} 40% removal efficiency Largest anthro: East Asia 33%, South Asia 27%	4300	11600	16.0	14.4
2050 A2	Sectors: Industrial processes 33% Power plant combustion 38% Residential/industrial fuel 29% Speciation: 45% Hg^{0}, 47% Hg^{II}, 8% Hg^{P} 40% removal efficiency Largest anthro: East Asia 41%, South Asia 14%	3400	12000	15.6	14.2
2050 B1	Sectors: Industrial processes 31% Power plant combustion 49% Residential/industrial fuel 20% Speciation: 45% Hg^{0}, 50% Hg^{II}, 5% Hg^{P} Removal efficiency: 70% developed regions 52% developing regions Largest anthro.: East Asia 31%, South Asia 21%	1900	9700	11.9	10.9
2050 B2	Sectors: Industrial processes 29% Power plant combustion 51% Residential/industrial fuel 20% Speciation: 43% Hg^{0}, 52% Hg^{II}, 5% Hg^{P} Removal efficiency: 70% developed regions 52% developing regions Largest anthro: East Asia 34%, South Asia 22%	2200	10300	12.7	11.6

[a]From Streets et al. (1)

Ocean Evasion

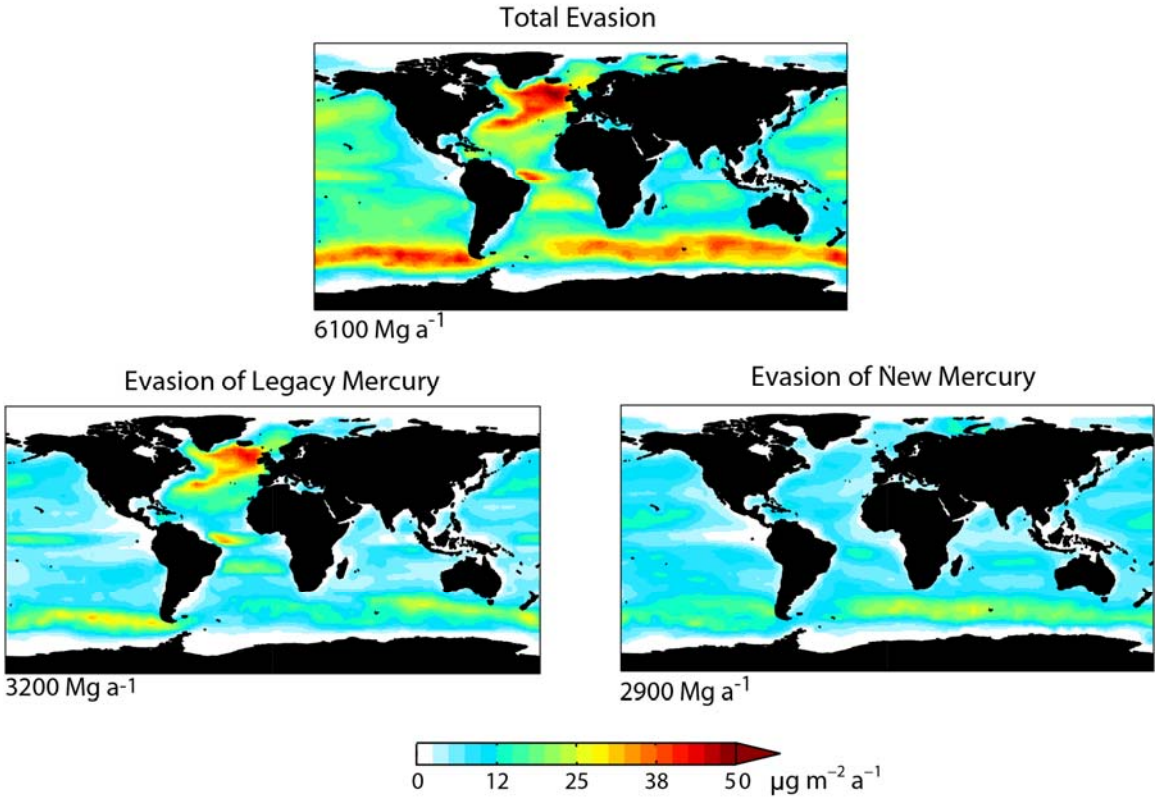

SI Figure 2 Gross evasion of mercury from the surface ocean to atmosphere divided into components from fast re-emission of recently deposited mercury and upwelling of legacy mercury from subsurface waters.

Net Deposition for All Scenarios

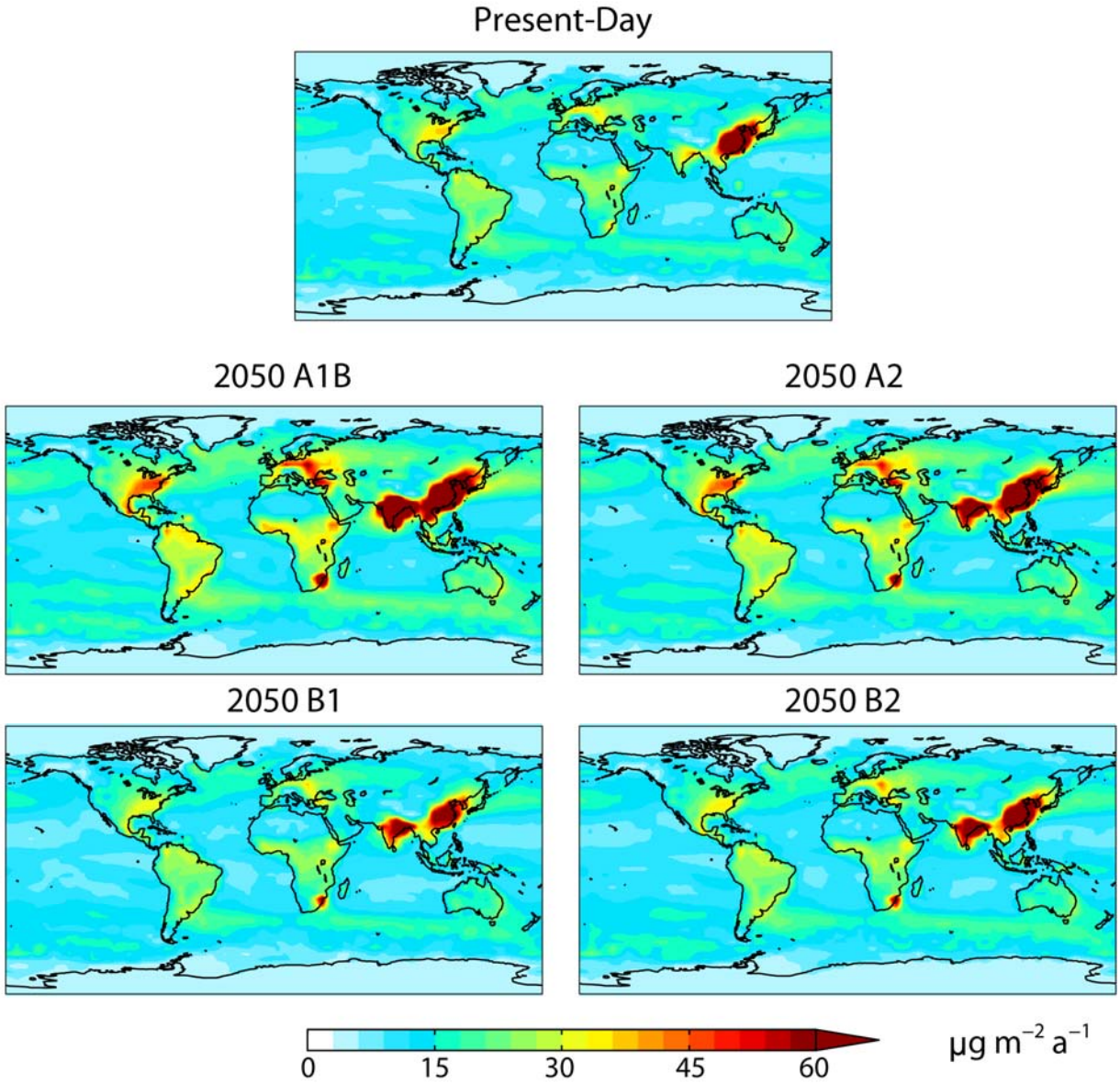

SI Figure 3 Global net deposition of mercury for the present-day and four IPCC scenarios.

Fraction of Deposition from Domestic Sources

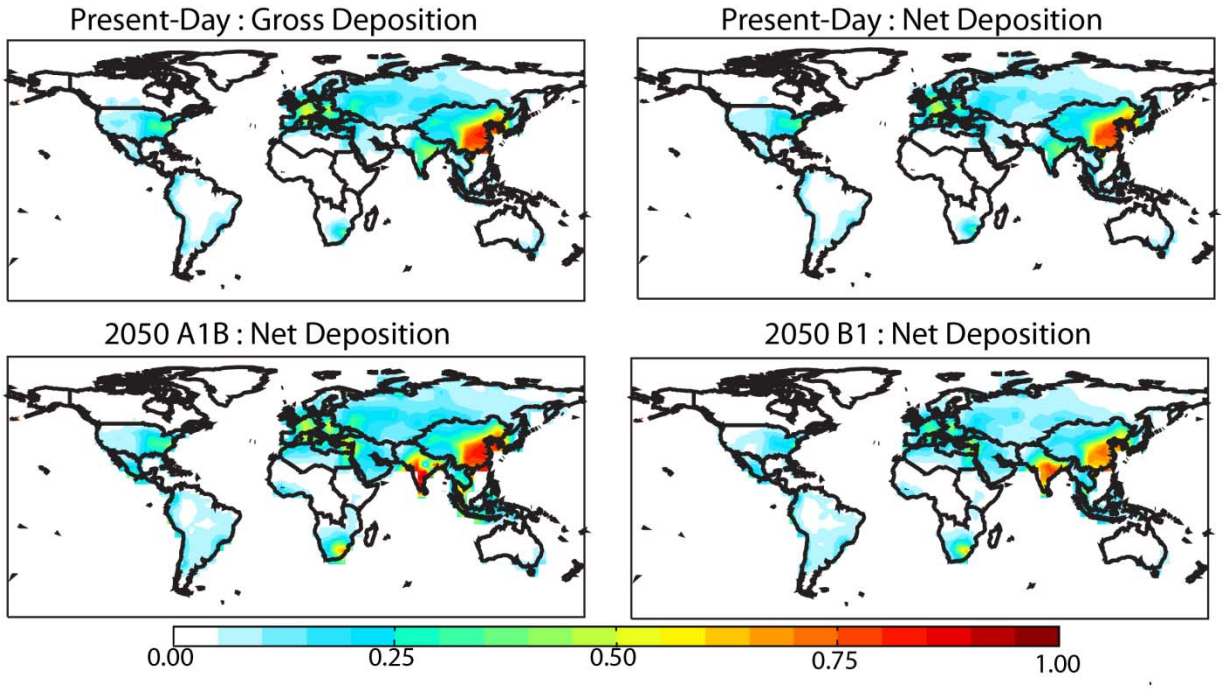

SI Figure 4 Fraction f_d of deposited mercury originating from anthropogenic sources within the same continental region indicated by heavy black lines. **Top panel:** F_d for gross and net deposition in the present-day. **Bottom panel:** F_d for net deposition in the 2050 A1B and B1 scenarios.

Influence Functions

We define the source-receptor influence function I_{ij} for mercury deposition as:

$$I_{ij} = \frac{D_{ij}}{E_i} \quad (1)$$

where D_{ij} is the net deposition flux to receptor region j from emissions in region i, and E_i is the total emission rate for region i. Examining influence functions enables us to evaluate where, gram-for-gram, emissions reductions would be most effective to reduce deposition to a given region.

The effective lifetime of Hg^0 taking into account reduction of Hg^{II} and recycling of deposited mercury is 9 months, still shorter than the timescale for interhemispheric exchange (~1 year (3)), meaning that Hg^0 is not globally well-mixed in the atmosphere. Previous studies have used observations of atmospheric variability, including the interhemispheric gradient, to estimate an Hg^0 lifetime of 0.5-2 years (4-6). This variability is well reproduced by GEOS-Chem, lending support to our lifetime estimates (7).

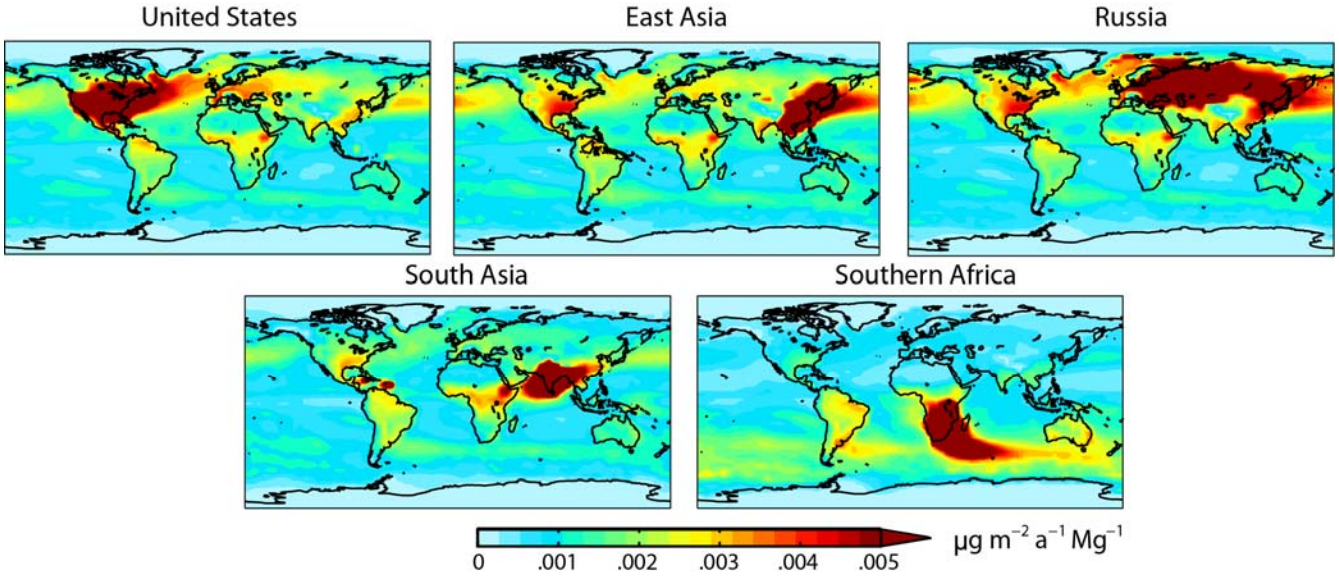

SI Figure 5 Influence functions for the present day for selected source regions: United States, East Asia, Russia, South Asia, and Southern Africa.

Regional Exporters and Importers of Anthropogenic Mercury

The ratio of anthropogenic mercury exported from a region and deposited elsewhere to the imported mercury deposited within the region from all external sources (R_E) is highly variable across regions and scenarios (Figure 6). In the present-day, East Asia has the greatest ratio of exports to imports (R_E=6) as expected due to its majority share of global anthropogenic emissions. The most importing regions (R_E < 0.2) are generally those which have the lowest emissions: West Africa, Canada, and Oceania. In the 2050 simulations, rapidly developing regions, such as South Asia, Central America, the Middle East, and Africa become more exporting in all scenarios, though may remain net importers. East Asia, Western Europe, Canada, and Oceania trend toward less exporting as the majority of any emissions increases are as Hg^{II} and deposit locally. The United States becomes more exporting in the A scenarios and more importing in the B scenarios, but remains a net importer in all future scenarios.

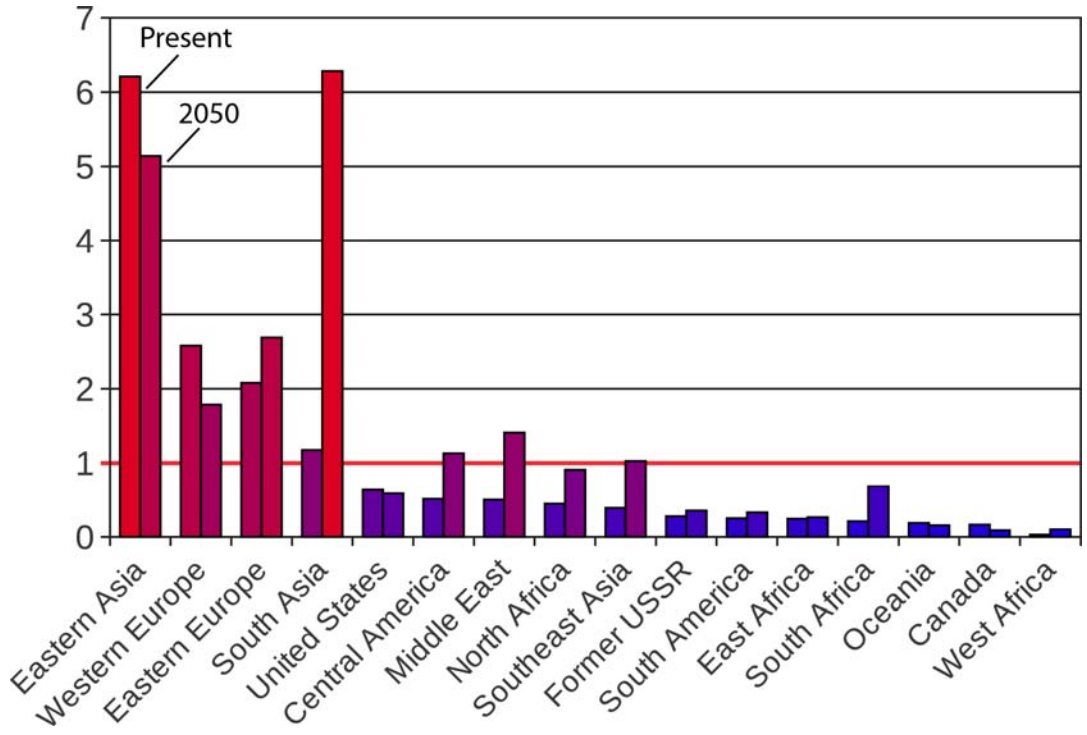

SI Figure 6 Ratio of exported to imported mercury deposition (R_E) by region for the present-day (first column) and average across all 2050 scenarios (second column). Red indicates regions that are net exporters (R_E>1) and blue indicates net importers (R_E<1).

Linear Regression Analysis

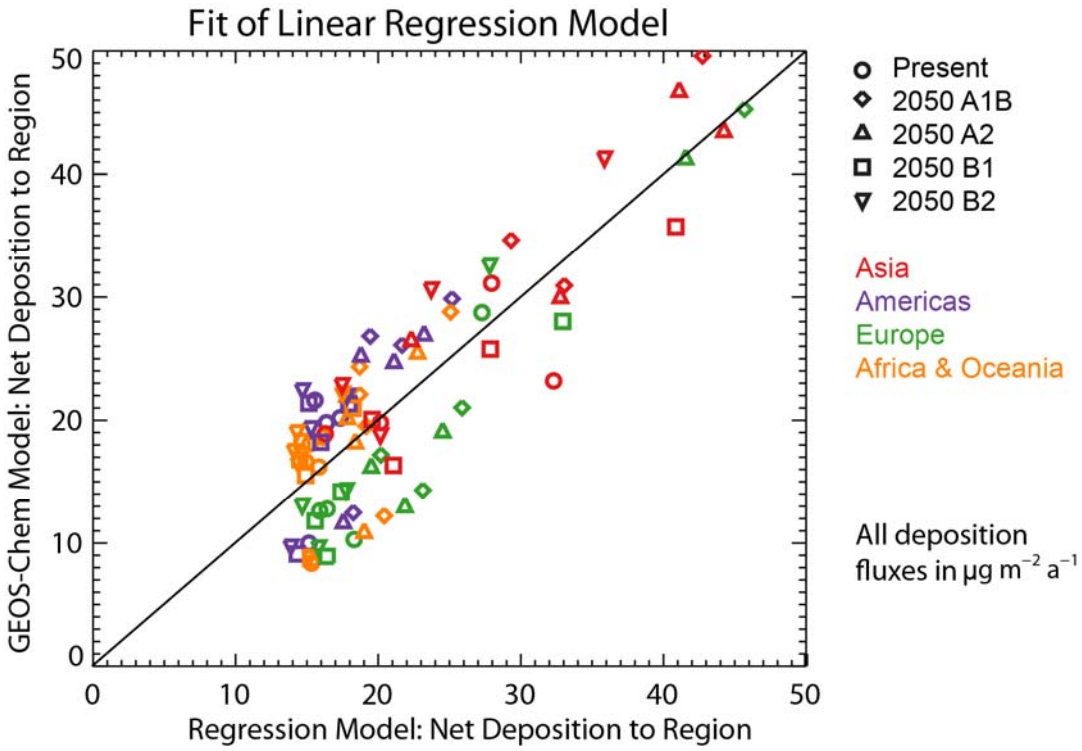

SI Figure 7 Fit of linear regression model for quick estimation of mean regional mercury deposition compared to deposition from the full atmosphere-land-ocean model. Regression model formula:

$$D_R = 0.39\, E_{R\,Hg}^{II} + 0.74\, E_{G\,Hg}^{0} + 10 \qquad (2)$$

All values in μg m^{-2} a^{-1}.

Model Sensitivity Analysis

The GEOS-Chem biogeochemical mercury model has been extensively evaluated with all available atmospheric and oceanic measurements in other studies (2,7-8). Here we evaluated the model's sensitivity to atmospheric redox reactions by comparing two alternate simulations to the base runs with Br as the major atmospheric oxidant and slow in-cloud reduction.

Total regional deposition in the simulation without in-cloud reduction differs by no more than 12% relative to the base simulation. Local differences may be up to 25%, with less deposition in remote areas of Antarctica and the Sahara, for example, and more deposition downwind of large Asian sources in Japan and Indonesia.

We found that modeled deposition using OH and O_3 as the major oxidant of Hg^0 instead of Br atoms does not change total deposition to any mid-latitude region by more than 12%. Above 60^o latitude, cold temperatures and the comparatively greater proportion of Br atoms, especially during springtime atmospheric mercury depletion events, enhance oxidation and deposition up to 78% compared to the OH/O_3 simulation. Net deposition in the OH/O_3 compared to the base simulation is 23% to the Arctic Ocean and72% less across Antarctica. At low latitudes, such as in northern Africa, southern Asia, and the Middle East, greater oxidation of Hg^0 in the OH/O_3 simulation increases modeled regional deposition up to 59% relative to the Br simulation. Our results are consistent with those from an inter-comparison of six mercury models for the Task Force on Hemispheric Transport of Air Pollution (HTAP), which found that modeled deposition was comparable in many regions globally but that polar regions are especially sensitive to model chemistry and transport (9).

Despite these differences in deposition magnitude in polar regions and at low latitudes, the composition of sources across the three sensitivity tests remains essentially unchanged (±2% and ±3%, respectively). This occurs because source contributions to the hemispheric atmospheric background dictate their relative abundance in deposition to remote regions rather than atmospheric oxidation. These results confirm that uncertainty in the magnitude of deposition in certain regions globally does not preclude an analysis of source contributions to deposition.

The extent to which scientific uncertainties affect our ability to reliably simulate deposition close to power plant and industrial sources in the eastern United States is of special concern to policy-makers. From our sensitivity analysis, we find that mean f_d for the eastern United States is 0.23, 0.25, or 0.20 for the base, no reduction, and OH/ O_3 oxidation cases, respectively. The relatively constrained range of modeled f_d bolsters the conclusion that both global and regional sources are important to deposition for the eastern U.S. A greater uncertainty is the proposed in-plume reduction of HgII. Observational studies have estimated that 10-90% of emitted Hg^{II} is reduced to Hg^0 over a period of >1 to 5 hours (10-12). This conversion would reduce the component of local deposition near sources, but the mechanism is currently unknown.

In the heavily impacted Ohio River Valley region, U.S. anthropogenic sources dominate the total changes in deposition in the 2050 scenarios. Anthropogenic deposition in this region decreases by 32% in the strictest emissions scenario considered here, but could decline even further if sorbent technologies, not currently commercially available, were implemented. Streets et al. (1) found that U.S. mercury emissions from power plants increased from 1996 to 2006. In the absence of regulation, continued growth in coal-fired power plants over the coming decades would likely increase U.S. mercury emissions and local deposition.

SI References

(1) Streets, D. G.; Zhang, Q.; Wu, Y. Projections of Global Mercury Emissions in 2050. *Environmental Science & Technology* **2009**, *43* (8), 2983.

(2) Soerensen, A. L.; Sunderland, E. M.; Holmes, C. D.; Jacob, D. J.; Yantosca, R. M.; Skov, H.; Christensen, J. H.; Strode, S. A.; Mason, R. P. An Improved Global Model for Air-Sea Exchange of Mercury: High Concentrations over the North Atlantic. *Environmental Science & Technology* **2010**, *44* (22), 8574.

(3) Jacob, D. J.; Prather, M. J.; Wofsy, S. C.; McElroy, M. B. Atmospheric distribution of Kr-85 simulated with a general-circulation model. *Journal of Geophysical Research-Atmospheres* **1987**, *92* (D6), 6614.

(4) Slemr, F.; Schuster, G.; Seiler, W. Distribution, speciation, and budget of atmospheric mercury. *J. Atmos. Chem.* **1985**, *3* (4), 407.

(5) Lin, C. J.; Pehkonen, S. O. The chemistry of atmospheric mercury: a review. *Atmospheric Environment* **1999**, *33* (13), 2067.

(6) Lindberg, S.; Bullock, R.; Ebinghaus, R.; Engstrom, D.; Feng, X. B.; Fitzgerald, W.; Pirrone, N.; Prestbo, E.; Seigneur, C. A synthesis of progress and uncertainties in attributing the sources of mercury in deposition. *Ambio* **2007**, *36* (1), 19.

(7) Holmes, C. D.; Jacob, D. J.; Corbitt, E. S.; Mao, J.; Yang, X.; Talbot, R.; Slemr, R. Global atmospheric model for mercury including oxidation by bromine atoms. *Atmospheric Chemistry and Physics* **2010**, *10* (24), 12037.

(8) Selin, N. E.; Jacob, D. J.; Yantosca, R. M.; Strode, S.; Jaegle, L.; Sunderland, E. M. Global 3-D land-ocean-atmosphere model for mercury: present-day versus preindustrial cycles and anthropogenic enrichment factors for deposition. *Global Biogeochemical Cycles* **2008**, *22* (2), GB2011.

(9) Travnikov, O.; Lin, C.-J.; Dastoor, A.; Bullock, O. R.; Hedgecock, I. M.; Holmes, C. D.; Ilyin, I.; Jaegle, L.; Jun, G.; Pan, L.; Pongrueksa, P.; Ryzhkov, A.; Seigneur, C.; Skov, H. *Mercury: Global and Regional Modeling*, 2011.

(10) Lohman, K.; Seigneur, C.; Edgerton, E.; Jansen, J. Modeling mercury in power plant plumes. *Environmental Science & Technology* **2006**, *40* (12), 3848.

(11) Edgerton, E. S.; Hartsell, B. E.; Jansen, J. J. Mercury speciation in coal-fired power plant plumes observed at three surface sites in the southeastern US. *Environmental Science & Technology* **2006**, *40* (15), 4563.

(12) Ter Schur, A.; Caffrey, J.; Gustin, M.; Holmes, C.; Hynes, A.; Landing, B.; Landis, M.; Laudel, D.; Levin, L.; Nair, U.; Jansen, J.; Ryan, J.; Walters, J.; Schauer, J.; Volkamer, R.; Waters, D.; Weiss-Penzias, P. An integrated approach to assess elevated mercury wet deposition and concentrations in the southeastern United States. *10th International Conference on Mercury as a Global Pollutant* Halifax, NS, Canada, 2011.